Int. J. Electrochem. Sci., 7 **(2012)** 7503 - 7515

International Journal of
ELECTROCHEMICAL
SCIENCE
www.electrochemsci.org

Investigation on the Electrochemical Behaviour of Copper Under HSO_3^--containing Thin Electrolyte Layers

K. Xiao, C. F. Dong[*]**,** *H.Luo, Q. Liu, X. G. Li*

Corrosion and Protection Center, University of Science and Technology Beijing, Beijing, China; Key Laboratory for Corrosion and Protection (MOE), Beijing, P. R. China
[*]E-mail: cfdong@ustb.edu.cn

Received: 26 June 2012 / *Accepted:* 14 July 2012 / *Published:* 1 August 2012

The electrochemical behaviour of copper under HSO_3^--containing thin electrolyte layers (TEL) was investigated by using potentiodynamic polarization, electrochemical impedance spectroscopy (EIS) and scanning electronic microscope (SEM). The results indicate that the corrosion potential of copper E_{corr} shifts to noble values in the presence of thinner TEL. The anodic current decreases, as the thickness of TEL decreases, indicating that the thin electrolyte layer can somewhat inhibit anodic corrosion rate. When the thickness of TEL under the 200 and 100 μm, special hump region appeared which involve some anodic reactions, in the very low overpotential during cathodic process. Moreover, the shape of corrosion products incline transfer from round and flat to irregular shape with thin electrolyte layers thickness increasing.

Keywords: Copper; Polarization; EIS; Atmospheric Corrosion; Thin electrolyte layers

1. INTRODUCTION

Considering the good mechanical properties and corrosion resistance, copper has been widely applied into not only though the traditional way, like sculptures and monuments, but also via the contemporary purposes, like the application in integrated circuit and microelectronics devices. Regardless of its strong anti-corrosion ability, copper and copper alloys may suffer damage in various situations, for instance, the presence of SO_2 [1-3] may cause deteriorations and serious problems, especially to electronic materials and devices due to their naturally small dimensions [2]. It is said that SO_2 accelerated atmospheric corrosion primarily due to the strong depolarizing agent H_2SO_3 generated by adsorbing in water. Therefore, $NaHSO_3$ solutions can be used to simulate any industrial environment with SO_2. However, up to now, very limited investigations of copper in $NaHSO_3$ solutions reveals that more attempts should be put in this field to better understand the corrosion behaviour of

copper in an atmospheric environment containing SO_2.

Much research indicates that metal corrosion behaviour in atmospheric environments is significantly different from that in bulk solutions. Essentially, atmospheric corrosion is an electrochemical process occurring on a metal surface covered with TEL [4]. During the past decades, many investigations [5-18] have been carried out to study the corrosion behaviour of metals under TEL conditions. The thickness of TEL always has an obvious effect on the corrosion behaviour of a metal. A change in the thickness of the electrolyte layer affects a number of processes, such as the mass transport of dissolved oxygen, the accumulation of corrosion products, and so on[13-15]. Evans [8] stated in a neutral or an alkaline solution, that oxygen gas transport rate through the electrolyte layer controls the rates of cathodic reaction of metallic corrosion. The results given by Zhang [14] showed that the cathodic process of copper under 100~1132 μm TEL with a dilute electrolyte Na_2SO_4 reveal a limiting oxygen diffusion current, revealing a good agreement with Fick's diffusion law.

In addition, these limiting diffusion current increases with the decrease of TEL thickness, which means that by decreasing the thickness of TEL, oxygen transport rate through the electrolyte layer can be accelerated. However, they also indicated that there is a maximum value of oxygen reduction current during the drying period. This reveals that the oxygen reduction current will not always increase with decreasing the thickness of TEL. It will experience a peak, and then begin to decrease with the appearance of even thinner TEL (<100 μm). Liao[18] studied the corrosion behaviour of copper under chloride-containing TEL. The results demonstrated that the copper corrosion rate under the TELs increased with decreasing TEL thickness at the initial immersion stage (2 h). Though there has been some investigations focusing on electrochemical behaviour of copper under TEL, the oxygen reduction mechanism during the cathodic process is still unclear.

In this paper, using $NaHSO_3$ solution as an electrolyte, potentiodynamic polarization curves and EIS of copper under TEL were measured to analyze the influence of TEL thickness on corrosion behaviour of copper and the cathodic oxygen reduction mechanism under TEL, at the same time, the corrosion products were investigated by SEM.

2. EXPERIMENTAL

2.1 Materials and solution

Copper samples of dimensions 10 mm×10 mm×3 mm and of composition Cu 99.90% (weight percent) with Pb and Ni as the main impurities were used in experiments. After being with electrical contact, they were embedded by epoxy resin mounting, leaving an exposed area of 1.0 cm^2. Prior to electrolyte exposure, the samples were sequentially ground with silicon carbide emery paper up to 2000 grit, then rinsed with deionized water and alcohol and dried under cool air stream. Analytical-grade $NaHSO_3$ and triply distilled water were used for preparing the solution with concentration of 0.05 M.

2.2 The determination of the electrolyte thickness

The thickness of a thin electrolyte layers (TEL) was measured by a spindle of micrometer screw gauge soldered with a very fine platinum needle, fixed at a proper position right above the electrode, as shown in Fig.1.

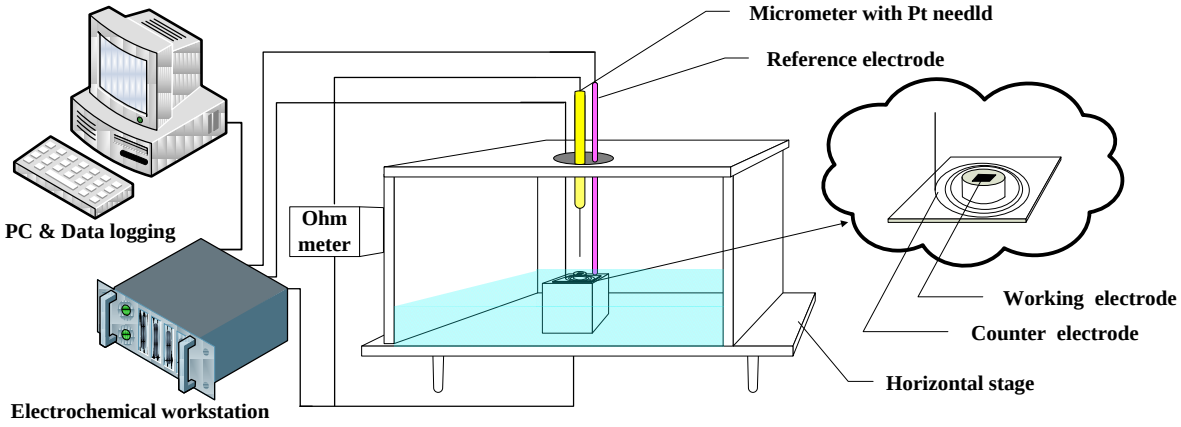

Figure 1. The schematic diagram of the device to control the electrolyte thickness on top of the sample.

In addition, a syringe was used to remove or add the electrolyte through the hole of the lid carefully to form the needed electrolyte layer thickness above the electrode. Slowly adjusted the platinum needle towards the electrode through micrometer screw gauge, when the platinum needle touched the electrolyte surface, the reading of ohmmeter sharply decreased to zero. Note down the reading of micrometer. Then reverse the micrometer screw gauge to a height, also keep the reading. In this case, the thickness was calculated based on two readings of micrometer screw gauge with an accuracy of 1.0 μm. To keep the thickness of electrolyte layer constant during tests, a Perspex lid was used to cover the cell to minimize the evaporation-induced variation of TEL thickness.

2.3. Electrochemical measurements

A conventional three-electrode cell arrangement was used for the electrochemical measurements, with a saturated calomel electrode (SCE) and a platinum plate as reference and auxiliary electrode, respectively. The electrochemical tests were carried out on the Princeton Applied – VMP3 electrochemical test system at room temperature under naturally aerated conditions. All potentials stated here were referred to SCE.

Polarization measurements were carried out starting from a cathodic potential of -800 mV_{SCE} (vs. Open-circuit Potential) to an anodic potential of +600 mV_{SCE} with a scan rate 1 mV/s. According to the polarization curves, several potential was chosen for oxide film growth and impedance analyses. Films were gown at each potential for 1 h to insure that the system was in steady state. EIS was

measured under a sinusoidal excitation potential of 10 mV in the frequency range from 100 kHz to 50 mHz. Fittings of the EIS plots were made by using ZSimpWin software.

FEI Quanta250 environmental scanning electron microscope was applied to evaluate corrosion morphology of samples after polarization measurements.

3. RESULTS AND DISCUSSION

3.1 Thickness of TEL on the electrochemical behaviour

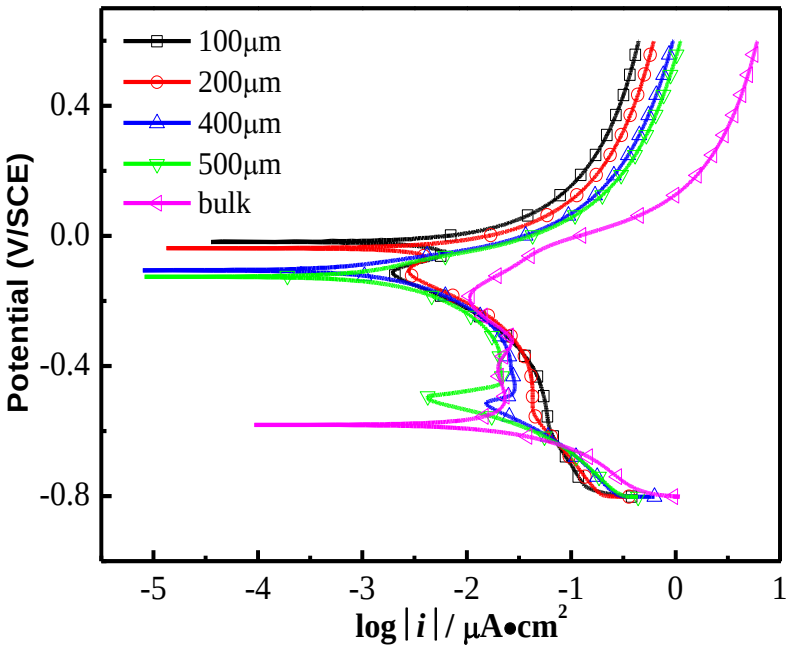

Figure 2. Potentiodynamic polarization curves measured for copper under layers of different thickness, electrolyte: 0.05 M $NaHSO_3$ solution, scan rate: 1 mVs^{-1}.

Table 1. Electrochemical polarization parameters of copper under different thickness of electrolyte layer, electrolyte: 0.05 M $NaHSO_3$ solution

Thickness of TEL/μm	E_{corr}/mV	i_{corr}/μA•cm^{-2}	β_c/mV	β_a /mV	β_a/β_c
100	-18.461	2.311	66.9	43.7	0.653214
200	-30.134	1.388	43.5	27.9	0.641379
400	-104.805	0.94	90.6	61.7	0.681015
500	-125.163	0.579	54	61.8	1.144444
bulk	-580.442	6.459	48.1	77.2	1.60499

Fig.2 shows the polarization curves measured for copper in 0.05 M $NaHSO_3$ under layers with different thicknesses. The corresponding electrochemical parameters obtained from potentiodynamic polarization curves such as corrosion potential (E_{corr}), corrosion current density (i_{corr}) and Tafel slopes

(β_a and β_c are the Tafel slopes for the cathodic and the anodic process, respectively) are shown in Table 1.

As can be seen in Fig.2 and Table 1, E_{corr} has the inclination to become nobler with the decrease in TEL thickness. As mentioned above, E_{corr} becomes to more positive values with the decrease in TEL thickness. It is said that the decrease in the thickness of TEL can accelerate cathodic process as well as inhibit the anodic process to some extent. However, considering the decrease in the values of β_a and the sharp increase in β_c in the presence of thinner electrolyte layer, it can be easily concluded that the TEL thickness acquires an even stronger influence on the cathodic process of copper. Therefore, it can be concluded that the acceleration of cathodic process is the main reason for the E_{corr} increasing.

As for the anodic part of these curves, under TEL, they have almost the same shape, indicating the similar reactions happened during anodic dissolution. However, the anodic current density is far smaller than that obtained in bulk. Additionally, with the decrease of TEL thickness, the anodic current density is even smaller. For example, at 200 mV_{SCE}, i_{bulk}=1.74 $mA \cdot cm^{-2}$, and while $i_{TEL=500\mu m}$=0.32 $mA \cdot cm^{-2}$, which is relatively small. This result disagrees with the result obtained by Liao [18] under chloride-containing TEL. However, these can be explained as follows, when under TEL condition, Evan [8] supposed that the diffusion of oxygen is much easier than that of in bulk. Therefore, the protective oxide film can be formed quickly, which increases the corrosion resistance, resulting in the drop of current density. Based on our results, the thinner the TEL, the quicker the protective film can be formed, and then the more decrease in current density. Actually after each experiment under TEL, there do is a very thin film on the sample surface. However, the bond between this film and sample surface is not strong enough, therefore, this film broken and floated on the solution surface when try to take the sample out after experiment.

As for the cathodic process, the current density shows a slight increase with the decrease in TEL thickness. It has been stated that, for most of the metals, such as iron and aluminum, the cathodic current density increased significantly with the decrease in TEL thickness, if the cathodic reaction rate was controlled by the reactant oxygen diffusion to the surface of the electrode [14, 19, 20]. Therefore, the cathodic process is not only controlled by oxygen diffusion, but also something else. Evans [8, 21] and Mansfeld [22, 23] proposed that corrosion rate mainly depends on the process of oxygen reduction for most metals and alloys under neutral or weak acid atmospheric environment. Therefore, this increase can own to the easy access to oxygen with the thinner and thinner electrolyte layer. Moreover, as can be seen, there are several peaks appearing on the cathodic part of the polarization curves.

3.2 Thickness of TEL on cathodic part of polarization curves

The potentiodynamic polarization curves for copper in naturally aerated 0.05 M $NaHSO_3$ are shown in Fig. 3. As can be seen, the cathodic current density of copper ranged from 10^{-4}~ 10^{-5} $A \cdot cm^{-2}$ for the one under TEL, which relatively agrees with that dominated by oxygen diffusion process [15]. On the other hand, for the one obtained in bulk, the cathodic current density is between 10^{-3}~10^{-4} $A \cdot cm^{-2}$. Therefore, it implied that the cathodic process of copper is dominated by the hydrogen evolution reaction (HER) in the bulk.

In order to thoroughly know the mechanism of the oxygen reduction reaction (ORR) for copper under TEL with electrolyte of 0.05 M $NaHSO_3$, according to the different characteristics artificially, the cathodic part are divided into four regions. Region 1(E<-0.55V_{SCE}), similarly to the polarization characteristics obtained in the bulk, cathodic current rising at relatively negative potentials between approximately -0.55 V_{SCE} and -0.8 V_{SCE} can be, obviously, agree with a result of the HER [24]. Region 2 (-0.55 V_{SCE}<E<-0.35 V_{SCE}) refers to oxygen diffusion limiting current at high catholic overpotentials; Region 3 (-0.35 V_{SCE} <E<-0.16 V_{SCE}) represents a mixed kinetic-diffusion control region; Region 4 (-0.16 V_{SCE} <E<-0.065 V_{SCE}) is defined as a hump phenomenon region where a maximum current density appears.

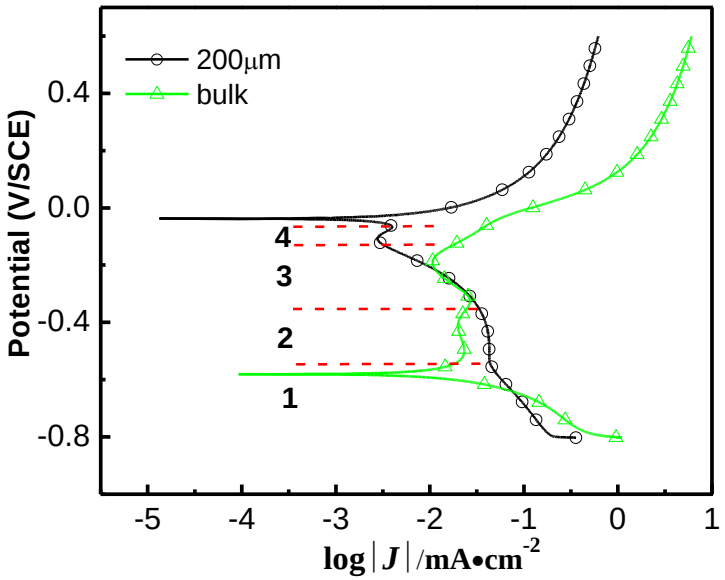

Figure 3. Polarization curves on the positive going sweep on copper under 200 μm TEL and bulk. Electrolyte: 0.05 M $NaHSO_3$, scan rate: 1 mVs^{-1}.

3.2.1 Oxygen reduction reaction in Region 2 and 3

Region 2 is the typical representative of oxygen reduction reaction (ORR). When the diffusion process is considered, the cathodic current for the corrosion metal electrode can be express by the following equation:

$$i_c = \frac{i_{corr}\exp(-\frac{\Delta E}{\beta_c})}{1-\frac{i_{corr}}{i_{lim}}[i_{corr}\exp(-\frac{\Delta E}{\beta_c})]} \qquad (1)$$

where i_c is the cathodic current, μm•cm^{-2}; i_{corr} the corrosion rate at the open circuit potential, μm•cm^{-2}; ΔE is the overpotential, V; β_c stands for the cathodic Tafel slope, and i_{lim} is the diffusion limiting current, μm•cm^{-2}.

Table 2. Impedance parameters of copper at potential of -0.54 V_{SCE} to -0.36 V_{SCE} under 200 μm TEL. Electrolyte: 0.05 M $NaHSO_3$.

E /V	R_s /Ωcm^2	Y^0_{dl} /μFcm^{-2}	n	$R_{o\text{-}ads}$ /Ωcm^2	$R_{t\text{-}O2}$ /Ωcm^2	$1/Y^0_w$ /Ωcm^2
-0.54	573.1	90.5	0.6725	8.01E+14	536.5	300.66
-0.52	579.1	98.37	0.6574	5.59E+14	666.2	394.94
-0.36	611.4	122	0.6527	4.63E+14	3485	979.43

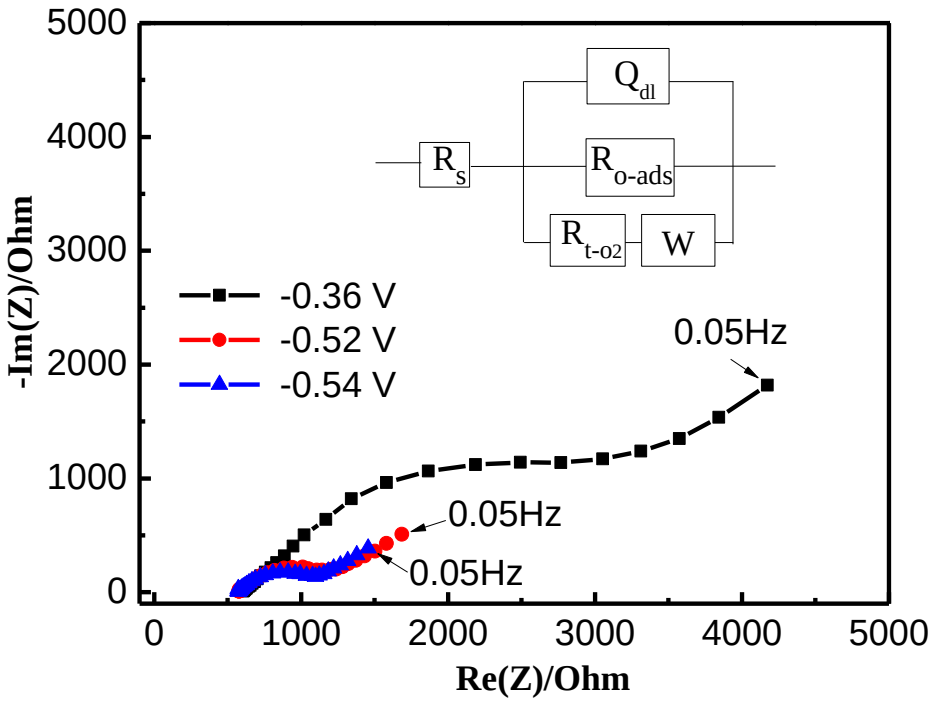

Figure 4. Under 200 μm TEL, Nyquist impedance spectra for copper obtained at different potentials (vs. SCE). Electrolyte: 0.05 M $NaHSO_3$, 100 kHz ~ 50 mHz. The insert is the equivalent circuit model.

When $i_{lim} >> i_{corr}$, the diffusion rate is fast, Eq. (1) becomes $i_c = i_{corr} \exp(-\Delta E/\beta_c)$. The electrode process is controlled only by the charge transfer process; when $i_{lim} = i_{corr}$, it becomes $i_c = i_{corr}$, which is the case that the cathodic process is totally controlled by the diffusion process. Therefore, considering i_{lim} (42.8 μA•cm^{-2}) only a bit larger than i_{corr} (2.020 μA•cm^{-2}), Region 2 is mixed controlled by charge transfer process and diffusion process. This can be verified by the impedance spectra shown in Fig.4. A high frequency (HF) capacitive loop and an obvious low frequency (LF) diffusion characteristic were observed. The HF capacitive loop is usually related to the double layer charging-discharging process, while the LF line is attributed to Warburg impedance, referring to diffusion process.

The impedance data is inferred according to the equivalent circuit insert in Fig.4. The fitted parameters are shown in Table 2. In the equivalent circuit, R_s is the solution impedance. $R_{O\text{-}ads}$ is the charge-transfer resistance of further reduction of the adsorbed intermediates, like H_2O_2. $R_{t\text{-}O2}$ is the charge transfer resistance of the direct 2e/4e ORR from oxygen molecules. *W* is the Warburg impedance.

In addition, *Q*, a constant phase element (CPE), denotes the double layer capacitance, describing the non-ideal behaviour of the capacitance, whose admittance and impedance are expressed as[25, 26]:

$$Z_{CPE} = \left(\frac{1}{Y^0}\right)(j\omega)^{-n} \qquad (2)$$

where Y^0 is the magnitude of *Q*, $\omega = 2\pi f$ stands for the angular frequency (in rad s^{-1}), *f* is the frequency of the applied signal, $j^2 = -1$ the imaginary number and *n*, is the exponential term. The value of *n* makes it possible to differentiate between the behaviour of an ideal capacitor (n=1) and of a constant phase element (n<1). When n=1, *Q* is equivalent to a capacitance; and for n=0.5, *Q* is equivalent to W; and to inductance when n= −1. The above equation provides information about the degree of non-idealibility in capacitive behaviour.

As can be seen from Table 2, in Region 2, $R_{t\text{-}O2} << R_{o\text{-}ads}$. Considering they are comparable in the equivalent circuit, it reveals that the direct 2e/4e ORR [27] is a fast step, having greater influence on the cathodic process. And according to Balakrishnana [28] and Vukmirovic [29], the 4e ORR should be the main reaction occurred in naturally aerated stagnant 0.05 M $NaHSO_3$ in Region 2.

$$O_2 + 4H^+ + 4e = 2H_2O \qquad (3)$$

$$O_2 + 2H^+ + 2e = H_2O_2 \qquad (4)$$

However, with the increase in the values of potential, $R_{t\text{-}O2}$ increases while $R_{o\text{-}ads}$ drops slightly. This reveals that at nobler potentials, reactions involving the adsorbed intermediates tend to happen. Moreover, though $1/Y^0_w < R_{t\text{-}O2}$ at more negative potentials, $1/Y^0_w$ increases with the potential, leading to$1/Y^0_w > R_{t\text{-}O2}$ at -0.36 V_{SCE}. This result not only reveals the appearance of a combined kinetic-diffusion control process, which agrees with the conclusion obtained from Eq. (1), but also indicates that the direct 4e ORR is the dominant reaction in Region 2.

When it comes to Region 3, cathodic current density decreases as the potential becomes less negative (as shown in Fig.3). The Nyquist plots in this region show that the spectrum diameter becomes larger while the LF diffusion characteristic wanes as the potential increases (as shown in Fig.5). The spectra were analyzed by the equivalent circuit inserted in Fig.6. Q_{ads} is related to the absorbed layer due to the intermediates during O_2 reduction reactions. The data obtained from fitting is listed in Table 3.

Table 3. Impedance parameters of copper at -0.3 V_{SCE} to -0.2 V_{SCE} in naturally aerated stagnant 0.05M $NaHSO_3$.

E /V	R_s /Ωcm^2	Y^0_{dl} /μFcm^{-2}	n	$R_{t\text{-}O2}$ /Ωcm^2	$R_{o\text{-}ads}$ /Ωcm^2	$1/Y^0_{ads}$ /Ω•cm^2	n_{ads}
-0.30	601.9	125.4	0.604	4280	1102	9.04E4	1
-0.20	620.3	151.3	0.605	6967	1025	2.07E4	0.865

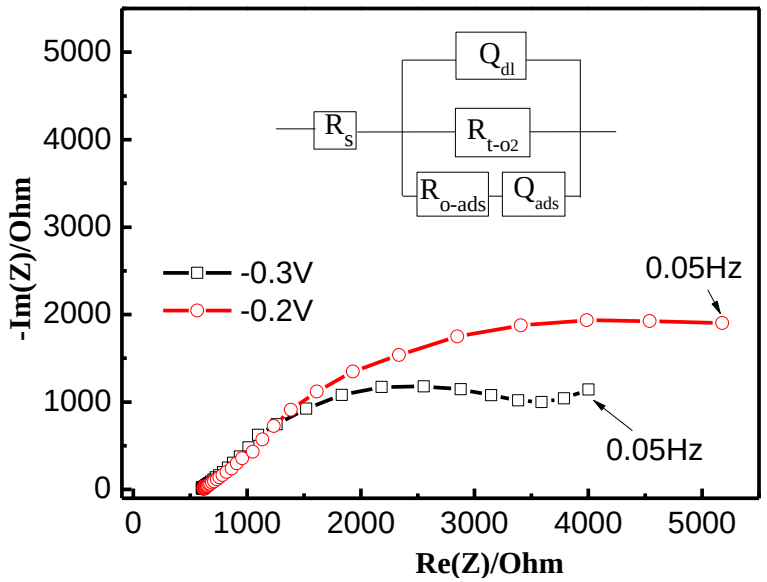

Figure 5. Under 200 μm TEL, Nyquist impedance spectra for copper in naturally aerated stagnant 0.05M $NaHSO_3$ at different potentials (vs. SCE), 100 kHz ~ 50 mHz. The insert is the equivalent circuit model.

Compare the data listed in Table 2 and 3, it is obvious that a sharply decrease in $R_{o\text{-}ads}$ occurs as the potential becomes nobler, resulting in $R_{o\text{-}ads}<R_{t\text{-}O2}$. Moreover, at -0.2 V_{SCE}, $R_{t\text{-}O2}$ was even bigger, almost as six times as $R_{o\text{-}ads}$, which inhibits the 4e ORR rate a lot. This may be due to the low overpotential, which provides less electrochemical drive. Nevertheless, the inhabitation of 4e ORR resulted in that O_2 prefers to be reduced via those reactions involving some intermediates, like HO^*, HO_2^* [30]. The big value of $1/Y^0_{ads}$ also reveals the considerable involvement of absorbed intermediates during ORR process in this potential Region. Considering what has stated above, in region 3, the ORR is essentially though the reactions involving some absorbed intermediates.

3.2.2 Hump phenomenon in Region 4

Region 4(-0.16V_{SCE}<E<-0.065 V_{SCE}) is a complex and distinctive region. It appears only when the thin electrolyte layer is no more than 200 μm as can be concluded from polarization curves in Fig.2. Another characteristic should be mentioned in this region is that the current density reaches a

minimum value of -2.82 μA•cm^{-2} at -0.11 V_{SCE} and then increases with potential, reaching a maximum value of -3.97 μA•cm^{-2} at -0.07 V_{SCE}, as can be seen in Fig. 3.

Ghandehari [31] stated that this hump phenomenon can be explained by the cathodic layer consisted of the intermediates appearing during ORR and absorbed anions. However, schultze and Wippermann [32] supposed that this is because of the redeposition of copper ions via cathodic reduction, which is impossible for a freshly reduced copper surface at any considerable rate. Therefore, some references [31, 33, 34] gave another explanation: in this region, anodic reaction happens due to the very low cathodic overpotential. The reactions may occur are as follows:

$$Cu \Leftrightarrow Cu(I)_{ads} + e \quad (5)$$

$$Cu(I)_{ads} \Leftrightarrow Cu(I)^{*}_{ads} + e \quad (6)$$

$$Cu(I)^{*}_{ads} + Cu \Leftrightarrow Cu(II)_{sol} + Cu(I)_{ads} + 2e \quad (7)$$

where $Cu(I)_{ads}$ is an absorbed monovalent species of copper; $Cu(I)_{ads}^{*}$ is a catalytic dissolution intermediate.

Table 4. Under 200 μm TEL, impedance parameters of copper at -0.1 V_{SCE}, electrolyte: 0.05M $NaHSO_3$.

E/V	R_s/Ωcm^2	Y^0_{dl}/μF•cm^{-2}	n_{dl}	$R_{o\text{-}ads}$/Ω•cm^2	R_{al}/Ω•cm^2	L/H•cm^2
-0.1	615.8	927.3	0.4116	659.5	1054	4051

Fig. 6 presents the impedance diagrams obtained at -0.1 V_{SCE}. Clearly, the capacitive loop is relatively small, and inductance arc appeared which indicates adsorption occurs on the sample surface. The adsorption particles may be $Cu(I)_{ads}$ or others in the solution. Correspondingly, according to the equivalent circuit in Fig.6 (In which, R_{al} stands for resistance to anodic reaction, mainly the transfer resistance of Cu to $Cu(I)_{ads}$), the related impedance parameters are listed in Table 4.

The data given in Table 4 shows that though $R_{o\text{-}ads} < R_{al}$, the difference between the two resistance is not so much. Under this circumstance, the cathodic reactions were mainly those involving ORR intermediates, while the anodic reaction is critically in accordance with Eq.5.

As has been discussed above, it can clearly get the conclusion that under TEL, in the most part of cathodic polarization process, oxygen was directly reduced to H_2O through the 4e ORR. However, with the increase of potential, $R_{t\text{-}O2}$ becomes bigger and bigger, while on the other hand, $R_{o\text{-}ads}$ decreases, resulting in that the reactions involving oxygen intermediates become the main reduction way for oxygen, especially in the hump region. Besides, in the hump region, owning to the very low overpotential, some anodic reactions occurred, which can affect the behaviour of copper in this region.

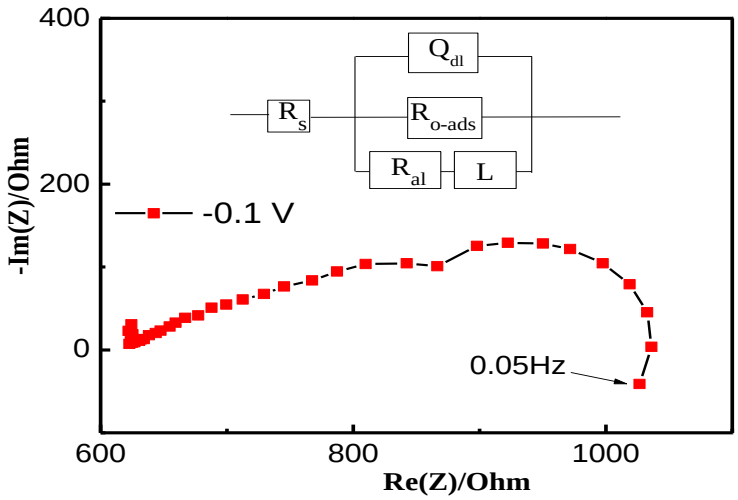

Figure 6. Under 200 μm TEL, nyquist impedance spectra for copper at -0.1 V_{SCE}, electrolyte: 0.05M $NaHSO_3$, 100 kHz ~ 50 mHz. The insert is the equivalent circuit model.

3.3 Thickness of TEL on surface morphology

Fig.7 provides the SEM of copper surface after polarization under TEL with various thicknesses. Obviously, as the increase in TEL thickness, corrosion products incline to transfer from round and flat with centre (obtained under 100 μm TEL, as shown in Fig.7a) to elliptic to irregular shape(obtained under 500 μm TEL, as shown in Fig.7c and d).

The difference in shape of corrosion products observed from different thicknesses TEL is due to the oxygen concentration in the TEL. When the sample is under a relatively thick TEL, like 500 μm, there might be not enough oxygen above the sample surface, because of short time for oxygen diffusing onto the sample surface. Alternatively, oxygen might unevenly distribute, leading the corrosion products to grow more at the place with plenty of oxygen, which makes corrosion product asymmetry. When the electrolyte layer thickness decreases, it is much easier for oxygen to reach sample surface, leading to more and more even distribution of oxygen. In this case, it is more possible for corrosion products growing symmetrically.

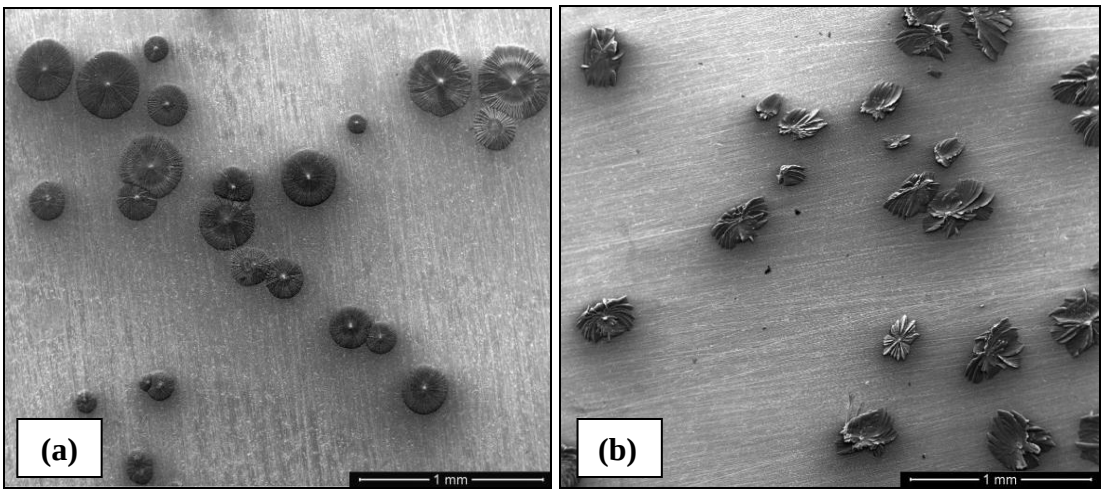

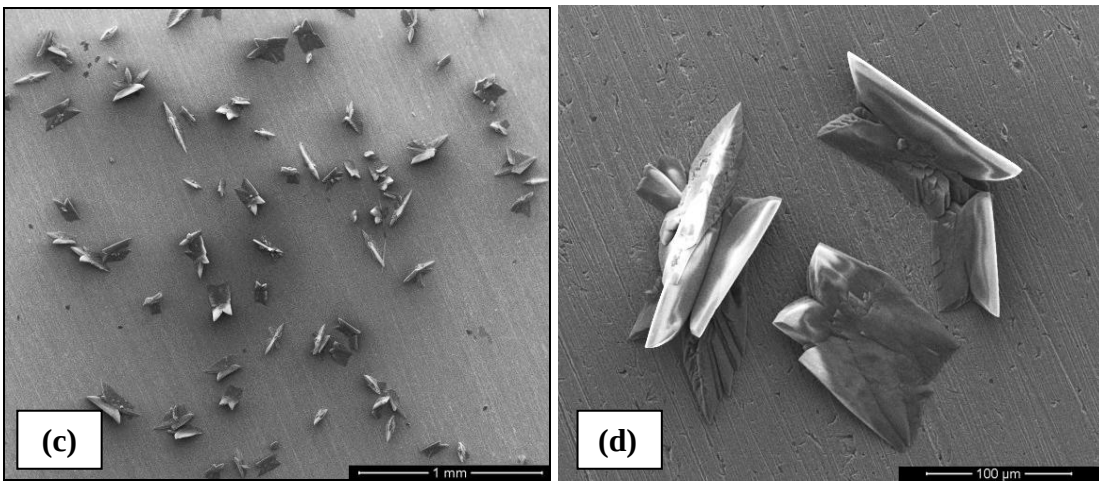

Figure 7. SEM of copper obtained under different thicknesses of TEL, electrolyte: 0.05 M NaHSO3, (a) 100 μm; (b)200 μm; (c)500 μm; (d) 500 μm, high magnification**.**

4. CONCLUSION

1. For copper, in 0.05 M $NaHSO_3$ solution, as TEL decreases its thickness, E_{corr} shifts to nobler values, and the anodic current density decreases obviously. The decrease in anodic current density indicates that the very thin electrolyte layer can somewhat inhibit corrosion rate.

2. Under TEL, in the most part of the cathodic polarization process, oxygen is directly reduced to H_2O. However, with the increase of potential, the reactions involving oxygen intermediates become the main reduction way for oxygen, especially in the hump region. Besides, some anodic reactions involved in the hump region.

3. As for the corrosion products, they are round and flat under 100 μm TEL, while under 500 μm TEL, with irregular shape. The difference in shape is due to the diffusion of oxygen.

ACKNOWLEDGEMENTS
This work is supported by the Fundamental Research Funds for the Central Universities (No. FRF-TP-11-006B) and the National Natural Science Foundation of China (No.50771020, No.51131005)

References

1. Z.Y. Chen, S. Zakipour, D. Persson and C. Leygraf, *Corrosion* 61(2005) 1022.
2. R. B. Comizzoli, R. P. Frankenthal and P. C. Milner and J. D. Sinclair, *Science* 234(1986) 340.
3. M. Watanabe, Y. Higashi and T. Ichino, *J. Electrochem. Soc.*150 (2003) B37.
4. N K. Nassau, A.E. Miller and T.E. Graedel, *Corros. Sci.* 27 (1987) 703.
5. M. Stratmann, H. Streckel, *Corros. Sci.* 30 (1990) 681.
6. M. Stratmann, H. Streckel, *Corros. Sci.* 30(1990) 697.
7. M. Stratmann , H. Streckel , K.T. Kim and S. Crockett, *Corros. Sci.* 30(1990) 715.
8. U.R. Evans, *Nature* 206 (1965) 980.

9. M. Keddam, A. Hugot-Le-Goff, H. Takenouti, D. Thierry and M.C. Arevalo, *Corros. Sci.* 33(1992) 1243.
10. T. Zhang, C.M. Chen, Y.W. Shao, G.Z. Meng, F.H. Wang, X.G. Li and C.F. Dong, *Electrochim. Acta* 53 (2008) 7921.
11. L.Y.Zheng, F.H. Cao, W.J.Liu, B.L.Jia and J.Q.Zhang, *Acta Metallurgica Sinica (English letters)* 23 (2010) 416.
12. W.J. Liu, F.H. Cao, B.L. Jia, L.Y. Zheng and J.Q. Zhang, C.N. Cao, X.G. Li, *Corros. Sci.* 52 (2010) 627.
13. A. Nishikata, Y. Ichihara and T. Tsuru, *Corros. Sci.* 37(1995) 897.
14. S.H. Zhang, S.B. Lyon, *Corros. Sci.* 35(1993) 713.
15. Y.L. Cheng, Z. Zhang, F.H. Cao, J.F. Lia, J.Q. Zhang, J.M. Wang and C.N. Cao, *Corros. Sci.* 46 (2004) 1649.
16. S.H. Zhang, S.B. Lyon, *Corros. Sci.* 36 (1994) 1289.
17. S.H. Zhang, S.B. Lyon, *Corros. Sci.* 36 (1994) 1309.
18. X. N. Liao, F. H. Cao, L. Y. Zheng, W. J. Liu, A. N. Chen, J. Q. Zhang and C. A. Cao, *Corros. Sci.* 53 (2011) 3289.
19. Y. Y Shi, Z.Zhang, F. H. Cao and J. Q. Zhang, *Electrochim. Acta* 51 (2006) 4977.
20. A. Nishikata, F. Suzuki and T. Tsuru, *Corros. Sci.* 47 (2005) 2578.
21. U.R. Evans, An Introduction to Metallic Corrosion. 3rd edition ed. 1981: Edward Arnold 13.
22. F. Mansfeld, M.W. Kendig and S. Tsai, *Corros. Sci.* 22 (1982) 455.
23. F. Mansfeld, S. Tsai, *Corros. Sci.* 20(1980) 853.
24. G. Quartarone, M. Battilana, L. Bonaldo and T. Tortato, *Corros. Sci.* 50 (2008) 3467.
25. C.N.Cao, J.Q.Zhang, Introduction to Electrochemical Impedance Spectroscopy. 2002, Beijing: Science Press.
26. H. Ma, S. Chen, B. Yin, S. Zhao and X. Liu, *Corros.Sci.* 45 (2003) 867.
27. J.G. Speight, Lange's Handbook of Chemistry (16th Edition), McGraw-Hill.
28. K. Balakrishnan, V.K. Venkatesan, *Electrochim. Acta* 24 (1979) 131.
29. M. B. Vukmirovic, N. Vasiljevic, N. Dimitrov and K. Sieradzki, *J. Electrochem. Soc.*150 (2003) B10.
30. Y.H.Lu, H.B.Xu, J.Wang and X.F.Kong, *Electrochim. Acta* 54 (2009) 3972.
31. M.H. Ghandehari, T.N. Andersen and H. Eyring, *Corros.Sci.* 16 (1976) 123.
32. J.W.Schultze, K. Wippermann, *Electrochim. Acta* 32 (1987) 823.
33. G. Moretti, F. Guidi, *Corros.Sci.* 44 (2002) 1995.
34. A.H. Moreira, A.V. Bendetti, P.L. Cabotand and P.T.A. Sumodjo, *Electrochim. Acta* 38 (1993) 981.